Relaxed Optimal Power Flow in AC/DC Microgrids

Deepak Pullaguram, *Member, IEEE,* Tuncay Altun, *Student Member, IEEE,* Ramtin Madani, *Member, IEEE,* and Ali Davoudi, *Senior Member, IEEE*

***Abstract*—An optimal power flow (OPF) paradigm, that guarantees a global optimal solution, is proposed for hybrid AC/DC microgrids. A meticulous model of the interlinking converter (IC) is developed and integrated into the OPF problem formulation. The resulting formulation is capable of solving OPF of AC and DC subgrids in their standalone operations. A computationally-efficient parabolic relaxation method transforms the non-convex OPF model into a convex quadratic-constrained quadratic programming form. A sequential penalization method is applied to the relaxed OPF to achieve a global solution for the original formulation. A modified IEEE 14-bus system is emulated in a hardware-in-the-loop setup to validate the proposed framework with continuously-varying loads and IC switching status.**

***Index Terms*—AC/DC microgrids, Convex optimization, Optimal power flow, Parabolic relaxation, Sequential penalization.**

I. Introduction

AC/DC microgrids are frequently used in electrification of remote areas, shipboard power systems, electrified transportation fleets, and more-electric aircraft. Compared to standalone AC or DC microgrids, a hybrid microgrid has fewer power conversion stages as energy storage units, renewable sources, and power electronics converters can be directly integrated into the DC subgrid, and synchronous machines and power electronics inverters into the AC subgrid. The two subgrids are interconnected using bidirectional interlinking converters (ICs) [1]. This paper reexamines the classical non-convex optimal power flow (OPF) problem to minimize the generation cost subject to physical constraints for a hybrid AC/DC microgrid. Interior-point methods can solve the OPF problems in AC power systems [2], but could end up at a local optimum [3]. Convex relaxation methods, such as semidefinite programming (SDP) [4] and second-order conic programming (SOCP) [5], [6] methods, lift the variables of the OPF problem to higher dimensions and relax them to convexify the original problem [7], [8]. In AC systems, SDP and SOCP relaxations guarantee the exact solution under certain conditions, e.g., sufficient virtual phase-shifters [9], [10], weakly-cyclic networks [11], or radial networks when lower bounds on generation are disregarded [12], [13]. SDP and SOCP relaxation techniques are extended to DC systems in [14], [15].

Proper modeling of ICs maintains accurate active power balance and voltage relation between its AC and DC terminals. The interior-point method in [16] incorporates IC losses into the formulation of the objective function. The SDP-relaxed OPF in [17] lifts the voltage vector of the AC and DC systems to form a single semidefinite matrix, but this could make the formulation computationally expensive. Large resistances are added between AC and DC terminals of the IC for network connectivity, which could lead to numerical instabilities. Two separate semidefinite matrices for AC and DC networks are needed to mitigate these numerical challenges [18]. The SOCP-based OPF [19] accommodates the active power balance constraint at the IC terminal. In [17]–[19], the IC filter and transformers are modeled as a part of the AC subgrid. This complicates solving individual OPFs for either AC or DC subgrids when the ICs are disconnected. Moreover, the voltage phase-angle constraints, that enforce the active power constraint, have been ignored. These methods might not guarantee an optimal solution under all conditions, e.g., mesh networks with generation and angle constraints [13].

This paper details an improved IC model by considering the voltage phase-angle and magnitude constraints to respect the active and reactive power limits of the IC. This modeling framework is integrated into the OPF formulation for an AC/DC microgrid. The OPF for individual AC or DC subgrids, in standalone operations, is solved by incorporating the breaker status in the IC constraints. Subgrid voltages are lifted into two individual matrices to avoid the numerical challenges caused by the addition of large resistance terms. The resulting lifted OPF problem is solved using a parabolic relaxation technique that is computationally superior to other relaxation approaches [20]. This relaxation transforms the non-convex OPF problem into a convex quadratic-constraint quadratic programming (QCQP) OPF problem, making it suitable for the commercially available solvers. Further, sequential penalization is applied to the relaxed OPF problem to obtain a globally optimal solution irrespective of the system conditions.

The remainder of the paper is as follows: Section II provides a summary of notations used throughout this paper. Section III details the OPF problem formulation for a complete AC/DC microgrid along with a detailed IC modeling that considers the active power balance, voltage, and angle constraints. Section IV presents the lifting, relaxation, and penalization needed to achieve the global solution. In Section V, feasibility of the OPF is verified using a hardware-in-the-loop (HIL) setup for a modified IEEE 14-bus network under varying loads and the IC switching status that highlights standalone OPF operations. Section VI concludes the paper.

II. Notations

The real and complex numbers are represented by $\mathbb{R}$ and $\mathbb{C}$, respectively. The symmetric matrix and the complex hermitian matrix of size $n \times n$ are denoted by $\mathbb{S}^n$ and $\mathbb{H}^n$, respectively. Scalars are presented in italic lower case (a), vectors in bold-italic lower case ($\boldsymbol{a}$), and matrices in bold-italic upper case

The authors are with the Department of Electrical Engineering, The University of Texas, Arlington, 76019 USA (deepak.pullaguram@uta.edu, tuncay.altun@mavs.uta.edu, ramtin.madani@uta.edu, davoudi@uta.edu). This research is funded, in part, by the Office of Naval Research under award N00014-18-1-2186.

($\boldsymbol{A}$). $[\boldsymbol{a}]$ represents a diagonal matrix with the '$\boldsymbol{a}$' vector of diagonal terms. $\mathbf{1}^n$ indicates a vector of ones with size $n \times 1$. The real and imaginary parts of a complex number or matrix are defined by $\mathrm{Re}\{\cdot\}$ and $\mathrm{Im}\{\cdot\}$, respectively. $\mathrm{diag}\{\cdot\}$ indicates the diagonal element vector of a square matrix. The transpose and conjugate transpose of a matrix are defined by $(\cdot)^\top$ and $(\cdot)^*$, respectively. $|\cdot|$ indicates the absolute value of a vector or a scalar element. $\mathrm{tr}(\cdot)$ represents the trace of a matrix. The AC subgrid variables and parameters use diacritic symbol tilde ($\tilde{\cdot}$). Diacritic symbol bar ($\bar{\cdot}$) is issued for DC subgrid variables and parameters.

III. OPF Problem Formulation

A generalized schematic of a AC/DC microgrid, with AC and DC subgrids connected through one or more ICs, is shown in Fig. 1. The AC/DC microgrid has $\mathcal{N} = \tilde{\mathcal{N}} \bigcup \bar{\mathcal{N}}$ buses and $\mathcal{L} = \tilde{\mathcal{L}} \bigcup \bar{\mathcal{L}}$ lines, where $\tilde{\mathcal{L}} \subseteq \tilde{\mathcal{N}} \times \tilde{\mathcal{N}}$ and $\mathcal{L} \subseteq \mathcal{N} \times \mathcal{N}$. $\tilde{\mathcal{N}} = \{1, 2, ..., \tilde{n}\}$ and $\mathcal{N} = \{1, 2, ..., \bar{n}\}$ are sets of AC and DC buses. $(j, k) \in \tilde{\mathcal{L}}$ is a set of AC lines, and $(j, k) \in \bar{\mathcal{L}}$ is a set of DC lines. The microgrid consists of $\tilde{\mathcal{N}}_\mathrm{g} = \{1, 2, ..., \tilde{n}_\mathrm{g}\}$ and $\bar{\mathcal{N}}_\mathrm{g} = \{1, 2, ..., \bar{n}_\mathrm{g}\}$ AC and DC generating units, respectively, with quadratic generation cost coefficients. The total generating units are $\mathcal{N}_\mathrm{g} = \tilde{\mathcal{N}}_\mathrm{g} \bigcup \bar{\mathcal{N}}_\mathrm{g}$.

A. AC Subgrid

The AC subgrid has $\tilde{\mathcal{N}}$ buses, $\tilde{\mathcal{L}}$ lines, and $\tilde{\mathcal{N}}_\mathrm{g}$ generators. The complex apparent power for all $\tilde{n}_\mathrm{g}$ generators is $\tilde{\boldsymbol{s}}^\mathrm{g} = \tilde{\boldsymbol{p}}^\mathrm{g} + \mathrm{i}\tilde{\boldsymbol{q}}^\mathrm{g} \in \mathbb{C}^{\tilde{n}_\mathrm{g} \times 1}$, where $\tilde{\boldsymbol{p}}^\mathrm{g} \in \mathbb{R}^{\tilde{n}_\mathrm{g} \times 1}$ and $\tilde{\boldsymbol{q}}^\mathrm{g} \in \mathbb{R}^{\tilde{n}_\mathrm{g} \times 1}$ are the vectors of active and reactive power generation. A generator incidence matrix is defined as $\tilde{\boldsymbol{G}} \in \{0, 1\}^{\tilde{n}_\mathrm{g} \times \tilde{n}}$. The load demand at all $\tilde{n}$ buses is given by a complex vector $\tilde{\boldsymbol{d}} \in \mathbb{C}^{\tilde{n} \times 1}$. The complex bus admittance matrix is given by $\tilde{\boldsymbol{Y}} \in \mathbb{C}^{\tilde{n} \times \tilde{n}}$, and the voltage vector by $\tilde{\boldsymbol{v}} \in \mathbb{C}^{\tilde{n} \times 1}$. The $from$ and to admittance matrices are shown as $\vec{\tilde{\boldsymbol{Y}}}$, $\overleftarrow{\tilde{\boldsymbol{Y}}} \in \mathbb{C}^{\tilde{n} \times \tilde{n}}$, and their respective branch incidence matrices as $\vec{\tilde{\boldsymbol{L}}}$, $\overleftarrow{\tilde{\boldsymbol{L}}} \in \{0, 1\}^{\tilde{l} \times \tilde{n}}$.

The power and voltage constraints for OPF are formulated by (1b)-(1g). The conservation of power in the complete AC subgrid is achieved using bus-injection power balance equality constraints in (1b). Constraints (1c) and (1d) ensure that the line flows in either directions are less than the maximum limit, $\tilde{f}^\mathrm{max}$. Active power generation vectors are bounded by $[\tilde{\boldsymbol{p}}^\mathrm{min}, \tilde{\boldsymbol{p}}^\mathrm{max}]$ through (1e). The constraint (1f) bounds the reactive power generation within $[\tilde{\boldsymbol{q}}^\mathrm{min}, \tilde{\boldsymbol{q}}^\mathrm{max}]$. The per-unit voltages are bounded within $[\tilde{\boldsymbol{v}}^\mathrm{min}, \tilde{\boldsymbol{v}}^\mathrm{max}]$ via (1g).

B. DC Subgrid

The DC subgrid has $\bar{\mathcal{N}}$ buses, $\bar{\mathcal{L}}$ lines, and $\bar{\mathcal{N}}_\mathrm{g}$ generators. $\bar{\boldsymbol{p}}^\mathrm{g} \in \mathbb{R}^{\bar{n}_\mathrm{g} \times 1}$ and $\bar{\boldsymbol{d}} \in \mathbb{R}^{\bar{n} \times 1}$ are the power generation and load demand vectors. The bus conductance matrix and voltage vector are denoted by $\bar{\boldsymbol{Y}} \in \mathbb{R}^{\bar{n} \times \bar{n}}$ and $\bar{\boldsymbol{v}} \in \mathbb{R}^{\bar{n} \times 1}$, respectively. The $from$ and to conductance matrices are $\vec{\bar{\boldsymbol{Y}}}$, $\overleftarrow{\bar{\boldsymbol{Y}}} \in \mathbb{R}^{\bar{n} \times \bar{n}}$. Define $from$ and to branch incidence matrices as $\vec{\bar{\boldsymbol{L}}}$, $\overleftarrow{\bar{\boldsymbol{L}}} \in \{0, 1\}^{\bar{l} \times \bar{n}}$, and the generator incidence matrix as $\bar{\boldsymbol{G}} \in \{0, 1\}^{\bar{n}_\mathrm{g} \times \bar{n}}$. The bus injection power balance is achieved by the equality constraint (1h). The power flow through resistive lines is limited by $\bar{f}^\mathrm{max}$ via constraints (1i) and (1j). The generation and bus voltages are limited within $[\bar{\boldsymbol{p}}^\mathrm{min}, \bar{\boldsymbol{p}}^\mathrm{max}]$ and $[\bar{\boldsymbol{v}}^\mathrm{min}, \bar{\boldsymbol{v}}^\mathrm{max}]$, using (1k) and (1l), respectively.

C. AC/DC Interlinking Converter

The AC and DC subgrids are connected through a set of ICs, $\mathcal{C} = \{1, 2, ..., n_\mathrm{c}\}$, with $\tilde{\mathcal{N}}_\mathrm{c} \subseteq \tilde{\mathcal{N}}$ and $\bar{\mathcal{N}}_\mathrm{c} \subseteq \bar{\mathcal{N}}$ as nodes to which ICs are connected on the AC and DC sides, respectively. The IC incidence matrices for AC and DC subgrids are defined as $\tilde{\boldsymbol{C}} \in \{0, 1\}^{n_\mathrm{c} \times \tilde{n}}$ and $\bar{\boldsymbol{C}} \in \{0, 1\}^{n_\mathrm{c} \times \bar{n}}$, respectively. $\tilde{\boldsymbol{s}}^\mathrm{c} \in \mathbb{C}^{\tilde{n}_\mathrm{c} \times 1}$ and $\bar{\boldsymbol{p}}^\mathrm{c} \in \mathbb{R}^{\bar{n}_\mathrm{c} \times 1}$ are the converter powers injected into the AC and the DC subgrids, respectively.

An IC incorporates a voltage-source converter (VSC) that connects to the AC subgrid through an LC filter and a transformer. The LC filter has z_f phase-reactor impedance and y_c shunt-filter susptance, as shown in Fig. 1. z_t indicates the transformer impedance. The AC and DC voltages across the VSC are correlated using its modulation index [21]:

$$|\tilde{v}_l| \leq \sqrt{\frac{3}{2}} m \bar{v}_i = c_m \bar{v}_i, \tag{3}$$

where m is the maximum modulation index (≈ 1). ICs control the power flow directly by controlling the active power flow or, indirectly, by controlling the DC bus voltage. They also control the reactive power injection at the AC side. The VSC obeys the conservation of power [21]

$$\bar{p}^c_m + \tilde{p}_l = p^\mathrm{loss}, \tag{4}$$

where p^loss are its losses, and p^c_m is DC power injected by the m^{th} IC. $\tilde{p}_l$ and $\tilde{v}_l$ are the internal active power and voltage variables for the m^{th} IC connected between the AC subgrid (bus j) and the DC subgrid (bus i).

The VSC operating capacity is limited by its maximum allowable current flow, i^max_l [22], i.e.,

$$|\tilde{s}_l| = \left| \sqrt{\tilde{p}_l^2 + \tilde{q}_l^2} \right| \leq (|\tilde{v}_l|\, \tilde{\imath}^\mathrm{max}_l). \tag{5}$$

The active power flow from bus l to bus j is limited by the maximum allowable angle difference at any operating voltage magnitude, $\tilde{\theta}^\mathrm{max}$, between the bus l and bus j

$$\tilde{\theta}_{lj} \leq \tilde{\theta}^\mathrm{max}, \tag{6}$$

where, $\tilde{\theta}_{lj} = \angle \tilde{v}_l - \angle \tilde{v}_j = \angle \tilde{v}_l \tilde{v}^*_j$.

The reactive power flow is influenced by the voltage magnitudes for bus l and bus j [22]. The voltage at bus l is constrained due to the DC voltage at bus i. Enforcing the voltage constraints

$$\tilde{v}^\mathrm{min}_j \leq |\tilde{v}_j| \leq \tilde{v}^\mathrm{max}_j, \tag{7a}$$
$$\bar{v}^\mathrm{min}_i \leq |\bar{v}_i| \leq \bar{v}^\mathrm{max}_i, \tag{7b}$$

mandates the reactive power flow over the IC. The IC is modeled to hold the constraints (3)-(6) using AC variables ($\tilde{v}_j$, $\tilde{s}^\mathrm{c}_m$, $\tilde{\imath}_l$) and DC variables ($\bar{v}_i$, $\bar{p}^\mathrm{c}_m$). Accordingly, the following proposition is made.

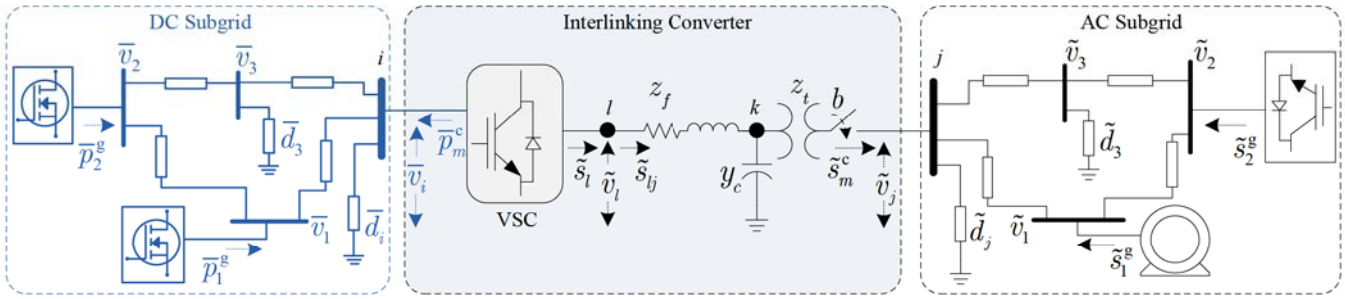

Fig. 1. AC/DC microgrid schematic with a detailed modeling of a DC subgrid, interlinking converter, and AC subgrid.

Original OPF formulation	Lifted OPF formulation
Objective function:	Objective function:
$\min \sum \tilde{\mathrm{f}}(\tilde{\boldsymbol{p}}^{\mathrm{g}}) + \sum \bar{\mathrm{f}}(\bar{\boldsymbol{p}}^{\mathrm{g}}) + \tilde{\imath}^{*}[\boldsymbol{\varrho}_2]\tilde{\imath} + \boldsymbol{\varrho}_1^{\top}\lvert\tilde{\imath}\rvert + \boldsymbol{\varrho}_0^{\top}\mathbf{1}^{\tilde{n}_{\mathrm{c}}}$ (1a)	$\min \sum \tilde{\mathrm{f}}(\tilde{\boldsymbol{p}}^{\mathrm{g}}) + \sum \bar{\mathrm{f}}(\bar{\boldsymbol{p}}^{\mathrm{g}}) + \boldsymbol{\varrho}_2^{\top}\tilde{\boldsymbol{o}} + \boldsymbol{\varrho}_1^{\top} abs\tilde{\imath} + \boldsymbol{\varrho}_0^{\top}\mathbf{1}^{\tilde{n}_{\mathrm{c}}}$ (2a)
AC subgrid constraints:	AC subgrid constraints:
$\tilde{\boldsymbol{G}}^{\top}\tilde{\boldsymbol{s}}^{\mathrm{g}} + \tilde{\boldsymbol{C}}^{\top}\tilde{\boldsymbol{s}}^{\mathrm{c}} = \tilde{\boldsymbol{d}} + \mathrm{diag}\{\tilde{\boldsymbol{v}}\tilde{\boldsymbol{v}}^{*}\tilde{\boldsymbol{Y}}^{*}\}$ (1b)	$\tilde{\boldsymbol{G}}^{\top}\tilde{\boldsymbol{s}}^{\mathrm{g}} + \tilde{\boldsymbol{C}}^{\top}\tilde{\boldsymbol{s}}^{\mathrm{c}} = \tilde{\boldsymbol{d}} + \mathrm{diag}\{\tilde{\boldsymbol{W}}\tilde{\boldsymbol{Y}}^{*}\}$ (2b)
$\lvert\mathrm{diag}\{\vec{\tilde{\boldsymbol{L}}}\tilde{\boldsymbol{v}}\tilde{\boldsymbol{v}}^{*}\vec{\tilde{\boldsymbol{Y}}}^{*}\}\rvert \le \tilde{\boldsymbol{f}}^{\max}$ (1c)	$\lvert\mathrm{diag}\{\vec{\tilde{\boldsymbol{L}}}\tilde{\boldsymbol{W}}\vec{\tilde{\boldsymbol{Y}}}^{*}\}\rvert \le \tilde{\boldsymbol{f}}^{\max}$ (2c)
$\lvert\mathrm{diag}\{\overleftarrow{\tilde{\boldsymbol{L}}}\tilde{\boldsymbol{v}}\tilde{\boldsymbol{v}}^{*}\overleftarrow{\tilde{\boldsymbol{Y}}}^{*}\}\rvert \le \tilde{\boldsymbol{f}}^{\max}$ (1d)	$\lvert\mathrm{diag}\{\overleftarrow{\tilde{\boldsymbol{L}}}\tilde{\boldsymbol{W}}\overleftarrow{\tilde{\boldsymbol{Y}}}^{*}\}\rvert \le \tilde{\boldsymbol{f}}^{\max}$ (2d)
$\tilde{\boldsymbol{p}}^{\min} \le \mathrm{Re}\{\tilde{\boldsymbol{s}}^{\mathrm{g}}\} \le \tilde{\boldsymbol{p}}^{\max}$ (1e)	$\tilde{\boldsymbol{p}}^{\min} \le \mathrm{Re}\{\tilde{\boldsymbol{s}}^{\mathrm{g}}\} \le \tilde{\boldsymbol{p}}^{\max}$ (2e)
$\tilde{\boldsymbol{q}}^{\min} \le \mathrm{Im}\{\tilde{\boldsymbol{s}}^{\mathrm{g}}\} \le \tilde{\boldsymbol{q}}^{\max}$ (1f)	$\tilde{\boldsymbol{q}}^{\min} \le \mathrm{Im}\{\tilde{\boldsymbol{s}}^{\mathrm{g}}\} \le \tilde{\boldsymbol{q}}^{\max}$ (2f)
$(\tilde{\boldsymbol{v}}^{\min})^2 \le \lvert\tilde{\boldsymbol{v}}\rvert^2 \le (\tilde{\boldsymbol{v}}^{\max})^2$ (1g)	$(\tilde{\boldsymbol{v}}^{\min})^2 \le \mathrm{diag}\{\tilde{\boldsymbol{W}}\} \le (\tilde{\boldsymbol{v}}^{\max})^2$ (2g)
DC subgrid constraints:	DC subgrid constraints:
$\bar{\boldsymbol{G}}^{\top}\bar{\boldsymbol{p}}^{\mathrm{g}} - \bar{\boldsymbol{C}}^{\top}\bar{\boldsymbol{p}}^{\mathrm{c}} = \bar{\boldsymbol{d}} + \mathrm{diag}\{\bar{\boldsymbol{v}}\bar{\boldsymbol{v}}^{\top}\bar{\boldsymbol{Y}}^{\top}\}$ (1h)	$\bar{\boldsymbol{G}}^{\top}\bar{\boldsymbol{p}}^{\mathrm{g}} - \bar{\boldsymbol{C}}^{\top}\bar{\boldsymbol{p}}^{\mathrm{c}} = \bar{\boldsymbol{d}} + \mathrm{diag}\{\bar{\boldsymbol{W}}\bar{\boldsymbol{Y}}^{\top}\}$ (2h)
$\lvert\mathrm{diag}\{\vec{\bar{\boldsymbol{L}}}\bar{\boldsymbol{v}}\bar{\boldsymbol{v}}^{\top}\vec{\bar{\boldsymbol{Y}}}^{\top}\}\rvert \le \bar{\boldsymbol{f}}^{\max}$ (1i)	$\lvert\mathrm{diag}\{\vec{\bar{\boldsymbol{L}}}\bar{\boldsymbol{W}}\vec{\bar{\boldsymbol{Y}}}^{\top}\}\rvert \le \bar{\boldsymbol{f}}^{\max}$ (2i)
$\lvert\mathrm{diag}\{\overleftarrow{\bar{\boldsymbol{L}}}\bar{\boldsymbol{v}}\bar{\boldsymbol{v}}^{\top}\overleftarrow{\bar{\boldsymbol{Y}}}^{\top}\}\rvert \le \bar{\boldsymbol{f}}^{\max}$ (1j)	$\lvert\mathrm{diag}\{\overleftarrow{\bar{\boldsymbol{L}}}\bar{\boldsymbol{W}}\overleftarrow{\bar{\boldsymbol{Y}}}^{\top}\}\rvert \le \bar{\boldsymbol{f}}^{\max}$ (2j)
$\bar{\boldsymbol{p}}^{\min} \le \bar{\boldsymbol{p}}^{\mathrm{g}} \le \bar{\boldsymbol{p}}^{\max}$ (1k)	$\bar{\boldsymbol{p}}^{\min} \le \bar{\boldsymbol{p}}^{\mathrm{g}} \le \bar{\boldsymbol{p}}^{\max}$ (2k)
$(\bar{\boldsymbol{v}}^{\min})^2 \le \lvert\bar{\boldsymbol{v}}\rvert^2 \le (\bar{\boldsymbol{v}}^{\max})^2$ (1l)	$(\bar{\boldsymbol{v}}^{\min})^2 \le \mathrm{diag}\{\bar{\boldsymbol{W}}\} \le (\bar{\boldsymbol{v}}^{\max})^2$ (2l)
Interlinking converter constraints:	Interlinking converter constraints:
$\boldsymbol{b}\tilde{\boldsymbol{s}}^{\mathrm{c}} = \boldsymbol{b}\mathrm{diag}\{[\boldsymbol{\gamma}]^{*}\tilde{\boldsymbol{C}}\tilde{\boldsymbol{v}}\tilde{\boldsymbol{v}}^{*}\tilde{\boldsymbol{C}}^{\top} + [\boldsymbol{\alpha}]^{*}\tilde{\boldsymbol{C}}\tilde{\boldsymbol{v}}\tilde{\boldsymbol{\imath}}^{*}\}$ (1m)	$\boldsymbol{b}\tilde{\boldsymbol{s}}^{\mathrm{c}} = \boldsymbol{b}\mathrm{diag}\{[\boldsymbol{\gamma}]^{*}\tilde{\boldsymbol{C}}\tilde{\boldsymbol{W}}\tilde{\boldsymbol{C}}^{\top} + [\boldsymbol{\alpha}]^{*}\tilde{\boldsymbol{C}}\tilde{\boldsymbol{v}}\tilde{\boldsymbol{\imath}}^{*}\}$ (2m)
$\boldsymbol{b}\boldsymbol{\varrho_1}\lvert\tilde{\boldsymbol{\imath}}\rvert = \boldsymbol{b}\left(\bar{\boldsymbol{p}}^{\mathrm{c}} + \mathrm{Re}\{[\boldsymbol{\eta}]\tilde{\boldsymbol{s}}^{\mathrm{c}}\} - \mathrm{diag}\{[\boldsymbol{\zeta}]\tilde{\boldsymbol{C}}\tilde{\boldsymbol{v}}\tilde{\boldsymbol{v}}^{*}\tilde{\boldsymbol{C}}^{\top}\} + [\boldsymbol{\sigma}]\lvert\tilde{\boldsymbol{\imath}}\rvert^2 - \boldsymbol{\varrho_0}\right)$ (1n)	$\boldsymbol{b}\boldsymbol{\varrho_1}\sqrt{\tilde{\boldsymbol{o}}} = \boldsymbol{b}\left(\bar{\boldsymbol{p}}^{\mathrm{c}} + \mathrm{Re}\{[\boldsymbol{\eta}]\tilde{\boldsymbol{s}}^{\mathrm{c}}\} - [\boldsymbol{\zeta}]\mathrm{diag}\{\tilde{\boldsymbol{C}}\tilde{\boldsymbol{W}}\tilde{\boldsymbol{C}}^{\top}\} + [\boldsymbol{\sigma}]\tilde{\boldsymbol{o}} - \boldsymbol{\varrho_0}\right)$ (2n)
$\lvert\tilde{\boldsymbol{\imath}}\rvert^2 \le (\tilde{\boldsymbol{\imath}}^{\max})^2$ (1o)	$\tilde{\boldsymbol{o}} \le \tilde{\boldsymbol{\imath}}^{\max 2}$ (2o)
$-\boldsymbol{\theta}^{\max} \le \angle([\boldsymbol{\varphi}]\lvert C\tilde{\boldsymbol{v}}\rvert^2 + [\boldsymbol{\rho}]\tilde{\boldsymbol{s}}^{\mathrm{c}^{*}}) \le \boldsymbol{\theta}^{\max}$ (1p)	$-\boldsymbol{\theta}^{\max} \le \angle([\boldsymbol{\varphi}]\mathrm{diag}\{\tilde{\boldsymbol{C}}\tilde{\boldsymbol{W}}\tilde{\boldsymbol{C}}^{\top}\} + [\boldsymbol{\rho}]\tilde{\boldsymbol{s}}^{\mathrm{c}^{*}}) \le \boldsymbol{\theta}^{\max}$ (2p)
$\mathrm{diag}\{[\lvert\boldsymbol{\alpha}\rvert^2]\tilde{\boldsymbol{C}}\tilde{\boldsymbol{v}}\tilde{\boldsymbol{v}}^{*}\tilde{\boldsymbol{C}}^{\top} + 2\mathrm{Re}\{[\boldsymbol{\kappa}]\tilde{\boldsymbol{C}}\tilde{\boldsymbol{v}}\tilde{\boldsymbol{\imath}}^{*}\}\} + [\lvert\boldsymbol{\beta}\rvert^2]\lvert\tilde{\boldsymbol{\imath}}\rvert^2 \le c_m^2\mathrm{diag}\{\tilde{\boldsymbol{C}}\tilde{\boldsymbol{v}}\tilde{\boldsymbol{v}}^{\top}\tilde{\boldsymbol{C}}^{\top}\}$ (1q)	$\mathrm{diag}\{[\lvert\boldsymbol{\alpha}\rvert^2]\tilde{\boldsymbol{C}}\tilde{\boldsymbol{W}}\tilde{\boldsymbol{C}}^{\top} + 2\mathrm{Re}\{[\boldsymbol{\kappa}]\tilde{\boldsymbol{C}}\tilde{\boldsymbol{v}}\tilde{\boldsymbol{\imath}}^{*}\}\} + [\lvert\boldsymbol{\beta}\rvert^2]\tilde{\boldsymbol{o}} \le c_m^2\mathrm{diag}\{\tilde{\boldsymbol{C}}\tilde{\boldsymbol{W}}\tilde{\boldsymbol{C}}^{\top}\}$ (2q)
$-\boldsymbol{bk} \le \tilde{\boldsymbol{s}}^{\mathrm{c}} \le \boldsymbol{bk},\ k \gg 1$ (1r)	$-\boldsymbol{bk} \le \tilde{\boldsymbol{s}}^{\mathrm{c}} \le \boldsymbol{bk},\ k \gg 1$ (2r)
$-\boldsymbol{bk} \le \bar{\boldsymbol{p}}^{\mathrm{c}} \le \boldsymbol{bk},\ k \gg 1$ (1s)	$-\boldsymbol{bk} \le \bar{\boldsymbol{p}}^{\mathrm{c}} \le \boldsymbol{bk},\ k \gg 1$ (2s)
$-\boldsymbol{bk} \le \tilde{\boldsymbol{\imath}} \le \boldsymbol{bk},\quad k \gg 1$ (1t)	$-\boldsymbol{bk} \le \tilde{\boldsymbol{o}} \le \boldsymbol{bk},\quad k \gg 1$ (2t)
	Lifted matrix constraints:
	$\tilde{\boldsymbol{W}} = \tilde{\boldsymbol{v}}\tilde{\boldsymbol{v}}^{*}$ (2u)
	$\bar{\boldsymbol{W}} = \bar{\boldsymbol{v}}\bar{\boldsymbol{v}}^{\top}$ (2v)

Proposition 1. *For an IC shown in Fig. 1, given $\tilde{v}_j$ and $\tilde{s}_m^{\mathrm{c}}$, the equality constraints imposed by the active power of the VSC can be formulated as*

$$\bar{p}_m^{\mathrm{c}} + \mathrm{Re}\{\eta\tilde{s}_m^{\mathrm{c}}\} - \zeta\lvert\tilde{v}_j\rvert^2 = -\sigma\lvert\tilde{\imath}_l\rvert^2 + \varrho_1\lvert\tilde{\imath}_l\rvert + \varrho_0, \tag{8}$$

$$\tilde{s}_m^{\mathrm{c}} = \tilde{v}_j(\gamma\tilde{v}_j + \alpha\tilde{\imath}_l)^{*}. \tag{9}$$

The inequalities of the IC can be defined as

$$\lvert\tilde{\imath}_l\rvert^2 \le \tilde{\imath}^{\max 2}, \tag{10}$$

$$\lvert\alpha\rvert^2\lvert\tilde{v}_j\rvert^2 + \lvert\beta\rvert^2\lvert\tilde{\imath}_l\rvert^2 + 2\mathrm{Re}\{\kappa\tilde{v}_j\tilde{\imath}_l^{*}\} \le c_m^2\bar{v}_i^2, \tag{11}$$

$$-(\pi - \angle\alpha) \le \angle(\varphi\lvert\tilde{v}_j\rvert^2 + \rho(\tilde{s}_m^{\mathrm{c}})^{*}) \le (\pi - \angle\alpha), \tag{12}$$

where

$$\alpha = \frac{1}{y_c z_t + 1},\ \beta = \frac{y_c z_t z_f + z_t + z_f}{y_c z_t + 1},\ \gamma = \frac{-y_c}{y_c z_t + 1}$$

ϱ_2 is VSC on-state conduction loss coefficient, ϱ_1 represent the switching losses coefficient, and ϱ_0 is no-load loss of the VSC,

$$\eta = \frac{\alpha}{\alpha^{*}},\ \zeta = \frac{\alpha\gamma*}{\alpha^{*}},\ \sigma = \mathrm{Re}\{\beta\} - \varrho_2,\ \kappa = 2\alpha\beta^{*},$$

$$\varphi = \alpha - \frac{\beta\gamma}{\alpha},\ \textit{and}\ \rho = \frac{\beta}{\alpha}.$$

Proof. Few definitions are needed first:

Definition 1. the converter voltage, $\tilde{v}_l$, and the current injected into AC subgrid, $\tilde{i}_j$, can be defined in terms of $\tilde{v}_j$ and $\tilde{i}_l$ using passive elements $z_f,\ y_c$, and z_f

$$\begin{aligned}\begin{bmatrix}\tilde{v}_l\\ \tilde{i}_j\end{bmatrix} &\triangleq \frac{1}{y_c z_t+1}\begin{bmatrix}1 & y_c z_t z_f + z_t + z_f\\ -y_c & 1\end{bmatrix}\begin{bmatrix}\tilde{v}_j\\ \tilde{i}_l\end{bmatrix}\\ &\triangleq \begin{bmatrix}\alpha & \beta\\ \gamma & \alpha\end{bmatrix}\begin{bmatrix}\tilde{v}_j\\ \tilde{i}_l\end{bmatrix}.\end{aligned} \tag{13}$$

The apparent power injected into the bus j by the IC is

$$\tilde{s}^{\mathrm{c}}_m = \tilde{v}_j \tilde{i}^*_j = \gamma^* |\tilde{v}_j|^2 + \alpha^* \tilde{v}_j \tilde{i}^*_l. \tag{14}$$

This can be reformulated as

$$\tilde{v}_j \tilde{i}^*_l = \frac{1}{\alpha^*}(\tilde{s}^{\mathrm{c}}_m - \gamma^* |\tilde{v}_j|^2). \tag{15}$$

The apparent power supplied by the VSC at bus l is

$$\tilde{s}_l = \tilde{v}_l \tilde{i}^*_l = (\alpha\tilde{v}_j + \beta\tilde{i}_l)\tilde{i}^*_l = \alpha\tilde{v}_j i^*_l + \beta |\tilde{i}_l|^2. \tag{16}$$

Using (15),

$$\tilde{s}_l = \frac{\alpha}{\alpha^*}(\tilde{s}^{\mathrm{c}}_m - \gamma^* |\tilde{v}_j|^2) + \beta |\tilde{i}_l|^2). \tag{17}$$

Definition 2. The total conduction, switching, and no-load losses of a VSC is a quadratic function of its current ($\tilde{i}_l$) [23]

$$p^{\mathrm{loss}} \triangleq \varrho_2 |\tilde{i}_l|^2 + \varrho_1 |\tilde{i}_l| + \varrho_0. \tag{18}$$

From (4), (17), and (18), the IC power balance becomes

$$\bar{p}_i + \mathrm{Re}\{\frac{\alpha}{\alpha^*}(\tilde{s}^{\mathrm{c}}_m - \gamma^* |\tilde{v}_j|^2) + \beta |\tilde{i}_l|^2)\} = \varrho_2 |\tilde{i}_l|^2 + \varrho_1 |\tilde{i}_l| + \varrho_0. \tag{19}$$

Define the following coefficients

$$\eta \triangleq \frac{\alpha}{\alpha^*} = \frac{(y_c z_t + 1)^*}{y_c z_t + 1}, \tag{20a}$$

$$\zeta \triangleq \mathrm{Re}\left\{\frac{\alpha\gamma^*}{\alpha^*}\right\} = \mathrm{Re}\left\{\frac{(y_c z_t z_f + z_t + z_f)^*}{y_c z_t + 1}\right\}, \tag{20b}$$

$$\sigma \triangleq \mathrm{Re}\{\beta\} - \varrho_2 = \mathrm{Re}\left\{\frac{(y_c z_t z_f + z_t + z_f)}{y_c z_t + 1}\right\} + \varrho_2. \tag{20c}$$

Then, (19) can be reformulated as

$$\bar{p}_i + \mathrm{Re}\{\eta \tilde{s}^{\mathrm{c}}_m\} - \zeta |\tilde{v}_j|^2 = -\sigma |\tilde{i}_l|^2 + \varrho_1 |\tilde{i}_l| + \varrho_0. \tag{21}$$

To enforce the voltage relation (3) between AC and DC subgrids, consider the square of magnitude of $\tilde{v}_l$ from (13)

$$\begin{aligned}|\tilde{v}_l|^2 &= |\alpha\tilde{v}_j + \beta\tilde{i}_l|^2\\ &= (\alpha\tilde{v}_j + \beta\tilde{i}_l)(\alpha\tilde{v}_j + \beta\tilde{i}_l)^*\\ &= |\alpha\tilde{v}_j|^2 + |\beta\tilde{i}_l|^2 + ((\alpha\tilde{v}_j)(\beta^*\tilde{i}^*_l))^* + ((\alpha\tilde{v}_j)(\beta^*\tilde{i}^*_l)).\end{aligned} \tag{22}$$

As $x^* + x = 2\mathrm{Re}\{x\}$, and by defining $\kappa \triangleq 2\alpha\beta^*$, from (3) and (22), the voltage relation is imposed by the following inequality

$$|\alpha|^2 |\tilde{v}_j|^2 + |\beta|^2 |\tilde{i}_l|^2 + 2\mathrm{Re}\{\kappa\tilde{v}_j\tilde{i}^*_l\} \le c^2_m \bar{v}^2_i. \tag{23}$$

Definition 3. To obtain the voltage phase-angle constraints, the current flowing from bus l to bus j, $\tilde{i}_l$, is defined in terms of α, β, $\tilde{v}_l$, and $\tilde{v}_j$ as

$$\begin{aligned}\tilde{i}_l &= \frac{y_c z_t + 1}{y_c z_t z_f + z_t + z_f}\tilde{v}_l - \frac{1}{y_c z_t z_f + z_t + z_f}\tilde{v}_j\\ &= \beta^{-1}\tilde{v}_l - \alpha^{-1}\tilde{v}_j.\end{aligned} \tag{24}$$

Using this, the apparent power flow from bus l to bus j is

$$\tilde{s}_{lj} = \tilde{v}_l \tilde{i}^*_l = \tilde{v}_l(\beta^{-1}\tilde{v}_l - \alpha^{-1}\tilde{v}_j)^*. \tag{25}$$

From Fig. 1, it is evident that $\tilde{s}_l = \tilde{s}_{lj}$. The active power flow from bus l to bus j becomes

$$\tilde{p}_l = \tilde{p}_{lj} = \frac{|\tilde{v}_l|^2}{|\beta|}\cos(\angle\beta) - \frac{|\tilde{v}_l|\,|\tilde{v}_j|}{|\alpha|}\cos(\theta_{lj} + \angle\alpha). \tag{26}$$

Differentiating this power flow with respect to θ_{lj},

$$\left.\frac{d\tilde{p}_l}{d\theta_{lj}}\right|_{\theta_{lj}=\theta^{\max}} = \frac{|\tilde{v}_l|\,|\tilde{v}_j|}{|\alpha|}\sin(\theta_{lj} + \angle\alpha) = 0, \tag{27}$$

gives

$$\theta^{\max} = \pi - \angle\alpha. \tag{28}$$

To enforce this angle limit as a constraint, consider

$$\tilde{v}_l\tilde{v}^*_j = (\alpha\tilde{v}_j + \beta\tilde{i}_l)\tilde{v}^*_j = \alpha |\tilde{v}_j|^2 + \beta\tilde{i}_l\tilde{v}^*_j. \tag{29}$$

From (15),

$$\tilde{v}_l\tilde{v}^*_j = \alpha |\tilde{v}_j|^2 + \frac{\beta}{\alpha}(\tilde{s}^*_j - \gamma |\tilde{v}_j|^2). \tag{30}$$

Defining $\varphi \triangleq \alpha - \frac{\beta\gamma}{\alpha}$ and $\rho \triangleq \frac{\beta}{\alpha}$, from (6), (28) and (30), one has the voltage phase-angle limits as

$$-(\pi - \angle\alpha) \le \angle(\varphi |\tilde{v}_j|^2 + \rho\tilde{s}^*_j) \le (\pi - \angle\alpha). \tag{31}$$

This completes the proof of proposition 1. □

Using (8)-(12), it is convenient to integrate an IC model into OPF models of the AC and DC subgrids.

D. AC/DC Optimal Power Flow

The basic OPF of AC/DC microgrid is formulated as (1).

Definition 4. Functions $\tilde{\mathrm{f}}(\tilde{\boldsymbol{p}}^{\mathrm{g}})$ and $\bar{\mathrm{f}}(\bar{\boldsymbol{p}}^{\mathrm{g}})$, in the objective function (1a), are defined as

$$\tilde{\mathrm{f}}(\tilde{\boldsymbol{p}}^{\mathrm{g}}) \triangleq (\tilde{\boldsymbol{p}}^{\mathrm{g}})^\top[\tilde{\boldsymbol{a}}_2]\tilde{\boldsymbol{p}}^{\mathrm{g}} + \tilde{\boldsymbol{a}}_1^\top\tilde{\boldsymbol{p}}^{\mathrm{g}} + \tilde{\boldsymbol{a}}_0^\top\mathbf{1}^{\tilde{n}_{\mathrm{g}}}, \tag{32a}$$

$$\bar{\mathrm{f}}(\bar{\boldsymbol{p}}^{\mathrm{g}}) \triangleq (\bar{\boldsymbol{p}}^{\mathrm{g}})^\top[\bar{\boldsymbol{a}}_2]\bar{\boldsymbol{p}}^{\mathrm{g}} + \bar{\boldsymbol{a}}_1^\top\bar{\boldsymbol{p}}^{\mathrm{g}} + \bar{\boldsymbol{a}}_0^\top\mathbf{1}^{\bar{n}_{\mathrm{g}}}. \tag{32b}$$

$\tilde{\boldsymbol{a}}_2$, $\tilde{\boldsymbol{a}}_1$, and $\tilde{\boldsymbol{a}}_0$ are quadratic cost coefficients for AC generators. $\bar{\boldsymbol{a}}_2$, $\bar{\boldsymbol{a}}_1$, and $\bar{\boldsymbol{a}}_0$ are their DC counterparts.

The constraints corresponding to the active power balance between AC and DC subgrids of all ICs are enforced using (1n). Here, $\boldsymbol{b} \in \{0,1\}$ is a binary vector representing the IC breaker status. The other equality constraints (1m) ensures the apparent power balance of the converter internally. The constraint (1o) limits the current flowing through the VSC within its thermal current limit, $\tilde{\imath}^{\max}$. The AC terminal voltage of the VSC is limited by the DC voltage across the converter using (1q).

Remark 1. If the breaker status is $\boldsymbol{b} = 0$, constraints (1m), (1n), and (1r)-(1t) restrict $\tilde{\boldsymbol{s}}^c$, $\bar{\boldsymbol{p}}^c$ and $\tilde{\boldsymbol{i}}^c$ to zero, and the resulting formulation will be the AC and DC standalone OPF problems with their generation cost as objective functions.

IV. Lifting, Relaxation, and Penalization

A. Lifting

The OPF problem in (1) is non-convex and NP-hard due to the non-linear constraints (1b)-(1q) with non-linear components such as $\tilde{\boldsymbol{v}}\tilde{\boldsymbol{v}}^*$, $\bar{\boldsymbol{v}}\bar{\boldsymbol{v}}^\top$, $|\tilde{\boldsymbol{v}}|^2$, $|\bar{\boldsymbol{v}}|^2$, $\tilde{\boldsymbol{v}}\tilde{\boldsymbol{i}}^*$, and $|\tilde{\boldsymbol{i}}|^2$. Except for $\tilde{\boldsymbol{v}}\tilde{\boldsymbol{i}}^*$, all other terms can be linearized by lifting them to a higher dimension. The OPF in (1) is reformulated with the lifted variables in (2) and the following additional constraints

$$\tilde{\boldsymbol{W}} = \tilde{\boldsymbol{v}}\tilde{\boldsymbol{v}}^*, \quad \bar{\boldsymbol{W}} = \bar{\boldsymbol{v}}\bar{\boldsymbol{v}}^\top, \quad \sqrt{\tilde{\boldsymbol{o}}} = |\tilde{\boldsymbol{i}}|\,. \tag{33}$$

$\tilde{\boldsymbol{W}} \in \mathbb{H}^{\tilde{n}}$, $\bar{\boldsymbol{W}} \in \mathbb{S}^{\bar{n}}$, and $\tilde{\boldsymbol{o}} \in \mathbb{R}^{\tilde{n}_c \times 1}$ are lifted auxiliary variables. The non-convex nature of (1) is absorbed in (IV-A). Constraints (2m) and (2q) are still non-convex due to $\tilde{\boldsymbol{v}}\tilde{\boldsymbol{i}}^*$ term. To make the lifted problem (2) computationally tractable, all these non-convex constraints should be relaxed.

B. Parabolic Relaxation

A computationally-efficient parabolic relaxation method [20] is used to avoid the conic constraints. It converts the original non-convex problem into a convex QCQP problem, making it realizable by available optimization packages. The parabolic relaxation of (IV-A) is

$$|\tilde{v}_j + \tilde{v}_k|^2 \le \tilde{W}_{jj} + \tilde{W}_{kk} + (\tilde{W}_{kj} + \tilde{W}_{jk}) \ \forall (j,k) \in \tilde{\mathcal{L}} \ (34a)$$
$$|\tilde{v}_j - \tilde{v}_k|^2 \le \tilde{W}_{jj} + \tilde{W}_{kk} - (\tilde{W}_{kj} + \tilde{W}_{jk}) \ \forall (j,k) \in \tilde{\mathcal{L}} \ (34b)$$
$$|\tilde{v}_j + \mathrm{i}\tilde{v}_k|^2 \le \tilde{W}_{jj} + \tilde{W}_{kk} - \mathrm{i}(\tilde{W}_{kj} - \tilde{W}_{jk}) \ \forall (j,k) \in \tilde{\mathcal{L}} \ (34c)$$
$$|\tilde{v}_j - \mathrm{i}\tilde{v}_k|^2 \le \tilde{W}_{jj} + \tilde{W}_{kk} + \mathrm{i}(\tilde{W}_{kj} - \tilde{W}_{jk}) \ \forall (j,k) \in \tilde{\mathcal{L}} \ (34d)$$
$$|\tilde{v}_i|^2 \le \tilde{W}_{ii} \qquad \forall i \in \tilde{\mathcal{N}}, \ (34e)$$

$$|\bar{v}_j + \bar{v}_k|^2 \le \bar{W}_{jj} + \bar{W}_{kk} + (\bar{W}_{kj} + \bar{W}_{jk}) \ \forall (j,k) \in \bar{\mathcal{L}} \ (35a)$$
$$|\bar{v}_j - \bar{v}_k|^2 \le \bar{W}_{jj} + \bar{W}_{kk} - (\bar{W}_{kj} + \bar{W}_{jk}) \ \forall (j,k) \in \bar{\mathcal{L}} \ (35b)$$
$$|\bar{v}_i|^2 \le \bar{W}_{ii} \qquad \forall i \in \bar{\mathcal{N}}. \ (35c)$$

To relax the non-convex expression (2m), it is formulated as

$$\tilde{v}_j \tilde{i}_l^* = (\alpha_l^*)^{-1}(\tilde{s}_m^c - \tilde{W}_{jj}\gamma_l^*) \quad \forall m \in \mathcal{C}, j \in \tilde{\mathcal{N}}_c. \tag{36}$$

Then, the parabolic relaxation of (36) becomes

$$b_m |\tilde{v}_j + \tilde{i}_l|^2 \le b_m(\tilde{W}_{jj} + \tilde{o}_{ll} + \mathrm{Re}\{\alpha_l^{-1}((\tilde{s}_m^c)^* - \tilde{W}_{jj}\gamma_l)\}) \ (37a)$$
$$b_m |\tilde{v}_j - \tilde{i}_l|^2 \le b_m(\tilde{W}_{jj} + \tilde{o}_{ll} - \mathrm{Re}\{\alpha_l^{-1}((\tilde{s}_m^c)^* - \tilde{W}_{jj}\gamma_l)\}) \ (37b)$$
$$b_m |\tilde{v}_j + \mathrm{i}\tilde{i}_l|^2 \le b_m(\tilde{W}_{jj} + \tilde{o}_{ll} - \mathrm{Im}\{\alpha_l^{-1}((\tilde{s}_m^c)^* - \tilde{W}_{jj}\gamma_l)\}) \ (37c)$$
$$b_m |\tilde{v}_j - \mathrm{i}\tilde{i}_l|^2 \le b_m(\tilde{W}_{jj} + \tilde{o}_{ll} + \mathrm{Im}\{\alpha_l^{-1}((\tilde{s}_m^c)^* - \tilde{W}_{jj}\gamma_l)\}) \ (37d)$$
$$b_m |\tilde{i}_l|^2 \le b_m \tilde{o}_{ll}. \ (37e)$$

The active power constraint of IC, (2n), is relaxed as

$$\boldsymbol{b}\boldsymbol{\varrho_1}|\tilde{\boldsymbol{i}}| \le \boldsymbol{b}(\bar{\boldsymbol{p}}^c + \mathrm{Re}\{[\boldsymbol{\eta}]\tilde{\boldsymbol{s}}^c\} - [\boldsymbol{\zeta}]\mathrm{diag}\{\tilde{\boldsymbol{C}}\tilde{\boldsymbol{W}}\tilde{\boldsymbol{C}}^\top\} + [\boldsymbol{\sigma}]\tilde{\boldsymbol{o}} - \boldsymbol{\varrho_0}) \le \boldsymbol{b}\boldsymbol{\varrho_1}\sqrt{\tilde{\boldsymbol{o}}}. \tag{38}$$

To make (2q) convex, substitute (36) in (11)

$$|\alpha_l|^2 \tilde{W}_{jj} + |\beta_l|^2 o_{ll} + \mathrm{Re}\{\kappa_l(\alpha_l^*)^{-1}(\tilde{s}_m^c - \gamma_l^* \tilde{W}_{jj})\} \le c_m^2 \bar{W}_{ii} \quad \forall l \in \mathcal{C}, j \in \tilde{\mathcal{N}}_c, i \in \bar{\mathcal{N}}_c. \tag{39}$$

C. Sequential Penalization

The relaxed convex OPF problem given by (2a)-(2l), (2p), and (34)-(39) might not guarantee a feasible solution to the original problem in (1). Therefore, the lifted objective function is appended with a linear penalty function $g_{\tilde{\mu},\bar{\mu},\boldsymbol{y}_0}(\tilde{\boldsymbol{W}}, \bar{\boldsymbol{W}}, \tilde{\boldsymbol{o}}, \tilde{\boldsymbol{v}}, \bar{\boldsymbol{v}}, \tilde{\boldsymbol{i}})$ at a given initial condition $\boldsymbol{y}_0 = (\tilde{\boldsymbol{v}}_0, \bar{\boldsymbol{v}}_0, \tilde{\boldsymbol{i}}_0)$ and with penalty gains $\tilde{\mu}$, $\bar{\mu}$.

Definition 5. The linear penalty function is defined as

$$\begin{aligned} g_{\tilde{\mu},\bar{\mu},\boldsymbol{y}_0}(\tilde{\boldsymbol{W}}, \bar{\boldsymbol{W}}, \tilde{\boldsymbol{o}}, \tilde{\boldsymbol{v}}, \boldsymbol{v}, \tilde{\boldsymbol{i}}) \triangleq \\ \tilde{\mu}\ \mathrm{tr}\{\tilde{\boldsymbol{W}} - \tilde{\boldsymbol{v}}^*\tilde{\boldsymbol{v}}_0 - \tilde{\boldsymbol{v}}_0^*\tilde{\boldsymbol{v}} + \tilde{\boldsymbol{v}}_0^*\tilde{\boldsymbol{v}}_0\} + \\ \bar{\mu}\ \mathrm{tr}\{\bar{\boldsymbol{W}} - 2\bar{\boldsymbol{v}}^\top\bar{\boldsymbol{v}}_0 + \bar{\boldsymbol{v}}_0^\top\bar{\boldsymbol{v}}_0\} + \\ \tilde{\mu}(\tilde{\boldsymbol{o}}^\top\boldsymbol{1}^{n_c} - \tilde{\boldsymbol{i}}^*\tilde{\boldsymbol{i}}_0 - \tilde{\boldsymbol{i}}_0^*\tilde{\boldsymbol{i}} + \tilde{\boldsymbol{i}}_0^*\tilde{\boldsymbol{i}}_0). \end{aligned} \tag{40}$$

The AC/DC OPF problem is solved iteratively by updating the initial conditions in each iteration using the solution from the previous iteration until the stopping criteria is reached.

V. Hardware-in-the-Loop Validation

A. HIL Setup

The IEEE 14-bus system was modified to form an AC/DC microgrid as shown in Fig. 2. The lines and buses with the blue color represent the DC subgrid, and those with the black color represent the AC subgrid. DC lines are modified to be resistive. DC generators are DC sources interfaced with the distribution network using DC-DC converters (buses filled in red) with an output voltage of $1kV$. The AC generators are a mixture of conventional diesel generators (filled with black and red) and VSCs (filled with red) with the output voltage of 480V transformed to $7.2kV$ before connecting to the distribution line. Table I lists the AC and DC generational limits and cost coefficients. The DC subgrid is connected to the AC subgrid using two ICs through a LC filter ($z_f = 0.01 + 0.3958i$, $y_c = -0.0188i$) and $400V/7.2kV$ step-up isolating transformers ($z_t = 0.0424i$). The nominal operating voltages are considered as base values. The base powers for AC and DC subgrids are $1MVA$ and $1MW$, respectively. This microgrid has variable-impedance AC loads at buses 2, 3, 5, 9 and variable resistive DC loads at buses 1, 7. The complete DC system, along with both ICs, are emulated in one Typhoon HIL604 unit, and the AC system is emulated in the second unit. All the AC and DC sources employ droop control schemes (P-f and Q-V droops in the AC subgrid, and the P-V droop in the DC subgrid), which are realized using two dSPACE MLBx control boxes. A personal computer (PC) with a 8-core, 3.5GHz Xeon processor, and 64GB RAM provides the OPF solution using the MATLAB/CPLEX optimization tool. Ethernet communication between Typhoon HIL - PC - dSPACE control boxes shares the load and setpoint information, as shown in Fig. 3.

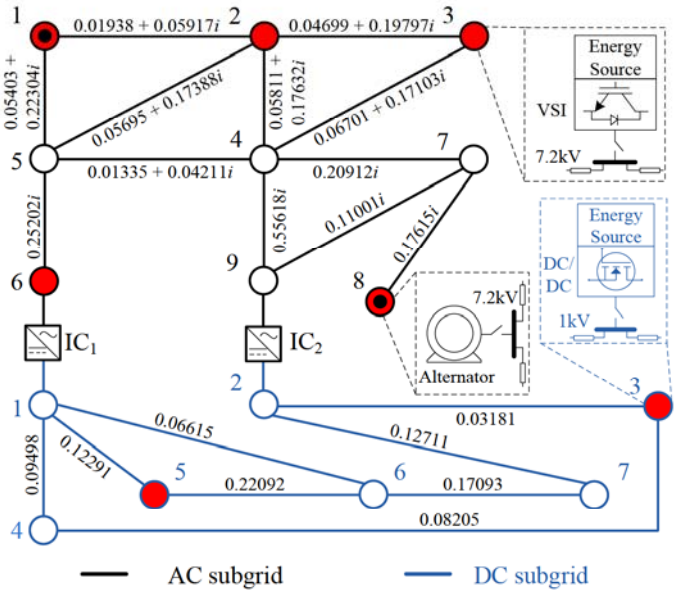

Fig. 2. The AC/DC microgrid system with AC and DC subgrids and the ICs.

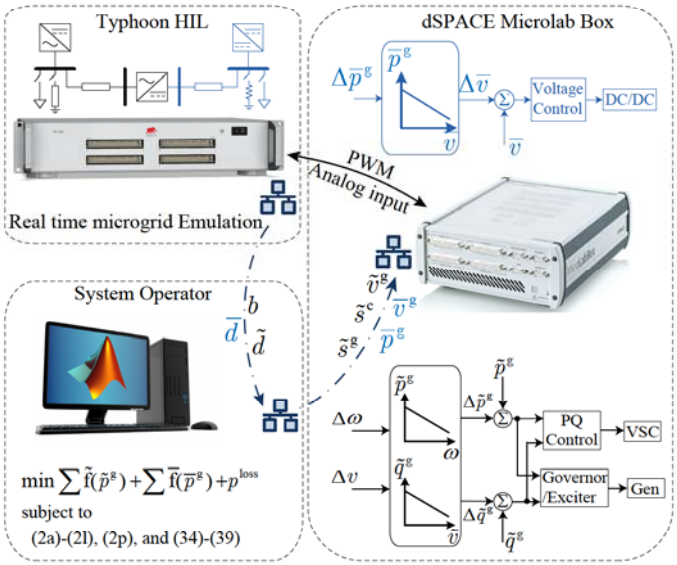

Fig. 3. HIL implementation of the AC/DC microgrid test system indicating the functionality of individual units and information flow.

TABLE I
GENERATORS COST COEFFICIENTS AND LIMITS

AC Generators							
Bus	$\tilde{a}_2$	$\tilde{a}_1$	$\tilde{a}_0$	$\tilde{p}^{\min}$	$\tilde{p}^{\max}$	$\tilde{q}^{\min}$	$\tilde{q}^{\max}$
1	0.04303	20	0	0	2.2	-0.20	0.40
2	0.25000	22	0	0	0.5	-0.30	0.20
3	0.05000	24	0	0	0.5	0.00	0.30
6	0.05000	24	0	0	0.5	-0.06	0.24
8	0.02000	23	0	0	2.2	-0.20	0.40
DC Generators							
Bus	$\bar{a}_2$	$\bar{a}_1$	$\bar{a}_0$	$\bar{p}^{\min}$	$\bar{p}^{\max}$		
1	0.10000	23	0	0	1.0		
2	0.08000	23	0	0	1.0		

B. Performance with and without OPF under Load Variation

Loads are varied at every $10s$ intervals as shown in Fig. 4(a),(d),(e) and 5(a),(d),(e). These variations are random and follow a poisson distribution nature. Any load variation was

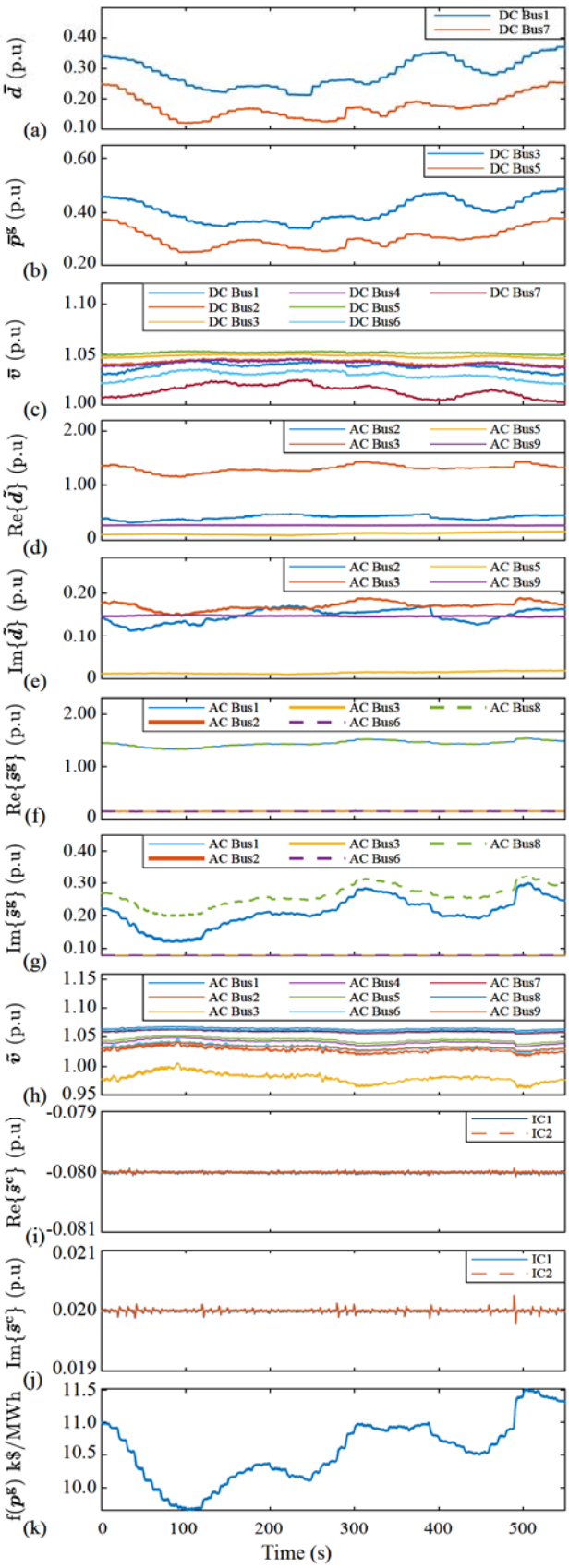

Fig. 4. Operation with droop control under varying load: (a) DC load variation, (b) DC generation, (c) DC system voltage, (d) AC system active load variation, (e) AC system reactive load variation, (f) AC system active power generation, (g) AC system reactive power generation, (h) AC system voltage, (i) IC active power flow, (j) IC reactive power flow, (k) total generation cost.

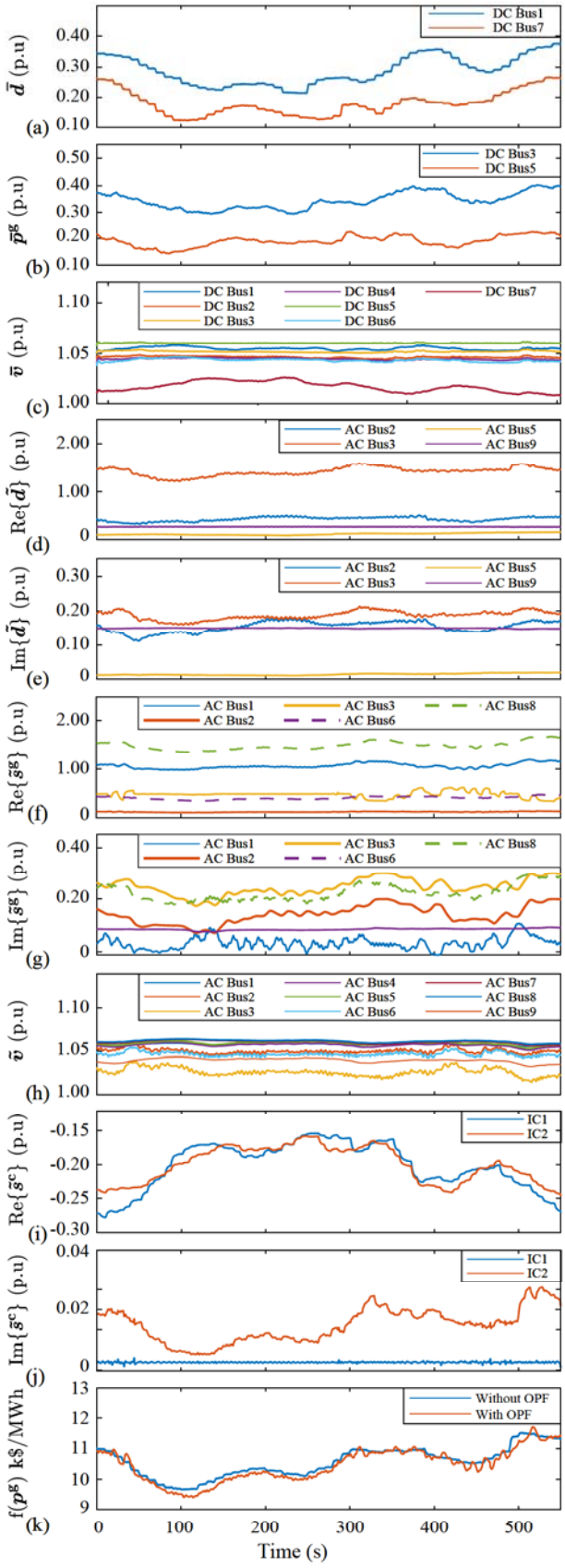

Fig. 5. Optimal operation with varying load: (a) DC load variation, (b) DC generation, (c) DC system voltage, (d) AC system active load variation, (e) AC system reactive load variation, (f) AC system active power generation, (g) AC system reactive power generation, (h) AC system voltage, (i) IC active power flow, (j) IC reactive power flow, and (k) total generation cost.

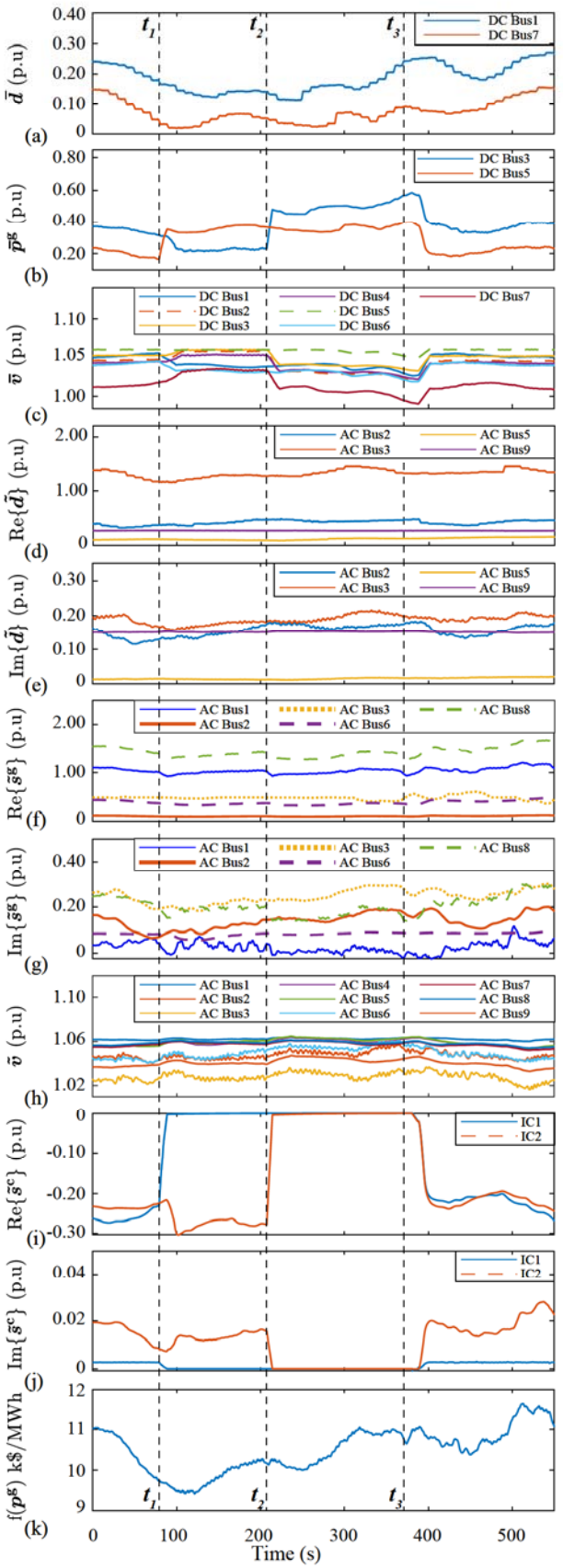

Fig. 6. Optimal operation with IC switching: (a) DC load variation, (b) DC generation, (c) DC system voltage, (d) AC system active load variation, (e) AC system reactive load variation, (f) AC system active power generation, (g) AC system reactive power generation, (h) AC system voltage, (i) IC active power flow, (j) IC reactive power flow, and (k) total generation cost.

proportionally distributed among all the sources per their droop coefficients. It can be seen that AC and DC voltages were held within their limits [0.94 p.u, 1.06 p.u] without (i.e., with droop alone) and with OPF, as shown in Fig. 4(h), (c) and 5(h), (c), respectively. With OPF, the DC generator with larger cost coefficients has reduced its generation (Fig. 5(b)) in comparison to the same scenario without OPF (Fig. 4(b)). Similarly, the active power generation from the AC generator at bus 2 is always held at zero (Fig. 5(f)) as it is the most costly generator. The overall generation cost with OPF is less than that without the OPF, as shown in Fig. 5(k). The average time taken to run the relaxed OPF, without penalization, was $0.346s$. Sequential penalization with penalty gains, $\tilde{\mu} = \bar{\mu} = 1000$, took an average time of $7.34s$.

C. OPF with IC Switching

This scenario evaluates the proposed IC modeling in the OPF of the AC/DC microgrid and its standalone AC and DC subgrids. Load variations are same as in the previous scenario. The optimization was continual without violating any constraints as depicted in Fig. 6. Until $t = t_1$, both the ICs were connected and the AC/DC microgrid operated at the optimized references provided by the OPF program running in parallel. At $t = t_1$, the IC_1 was disconnected from the AC subgrid, ($b_1 = 0$); This reduced the active and reactive powers of IC_1 to zero, i.e., $\tilde{s}_1^c = 0$, as seen in Fig. 6 (i),(j), thereby, $\bar{p}_1^c = 0$ due to (38). The optimization solver read system data along with the IC_1 status, and provided optimized references for DC generators, AC generators, and IC_2 as depicted in Fig. 6(b), (f), (g), (i) and (j). At $t = t_2$, the IC_2 was disconnected to separate AC and DC subgrids. Even in this standalone mode, the proposed optimization framework was able to individually solve the OPF problem for the AC and DC subgrids without modifying the problem formulation. At $t = t_3$, both the ICs were reconnected and formed the AC/DC microgrid. The optimzation solver read the system load along with the IC status, $\boldsymbol{b} = 1$, and provided the global optimal solution. Throughout this study, the AC and DC voltages are held within the limits, as shown in Fig. 6(c) and (h).

VI. Conclusion

An OPF method is elaborated for AC/DC microgrids. The detailed modeling of the IC, that bridges AC and DC subgrids, was integrated into the OPF formulation. Constraints on the voltage angle and magnitude satisfy the power balance and voltage relation across the AC and DC sides, and respect the active and reactive power limits of the IC. The resulting OPF problem offers individual optimal operating points for AC and DC subgrids. The hybrid OPF problem was relaxed using a computationally-efficient parabolic relaxation technique that transforms the original non-convex OPF to a convex QCQP problem. The relaxed problem was then solved using a sequential penalization technique to obtain a globally optimal solution. The proposed OPF paradigm is validated on a modified IEEE 14-bus testbed emulated in the HIL environment with varying loads and IC switching status.

References

[1] F. Nejabatkhah and Y. W. Li, "Overview of power management strategies of hybrid ac/dc microgrid," *IEEE Transactions on Power Electronics*, vol. 30, no. 12, pp. 7072–7089, Dec 2015.

[2] R. D. Zimmerman, C. E. Murillo-Sanchez, and R. J. Thomas, "Matpower: Steady-state operations, planning, and analysis tools for power systems research and education," *IEEE Transactions on Power Systems*, vol. 26, no. 1, pp. 12–19, Feb 2011.

[3] W. A. Bukhsh, A. Grothey, K. I. M. McKinnon, and P. A. Trodden, "Local solutions of the optimal power flow problem," *IEEE Transactions on Power Systems*, vol. 28, no. 4, pp. 4780–4788, Nov 2013.

[4] J. Lavaei and S. H. Low, "Zero duality gap in optimal power flow problem," *IEEE Transactions on Power Systems*, vol. 27, no. 1, pp. 92–107, Feb 2012.

[5] R. A. Jabr, "Radial distribution load flow using conic programming," *IEEE Transactions on Power Systems*, vol. 21, no. 3, pp. 1458–1459, Aug 2006.

[6] R. A. Jabr, R. Singh, and B. C. Pal, "Minimum loss network reconfiguration using mixed-integer convex programming," *IEEE Transactions on Power Systems*, vol. 27, no. 2, pp. 1106–1115, May 2012.

[7] S. H. Low, "Convex relaxation of optimal power flow—part I: Formulations and equivalence," *IEEE Transactions on Control of Network Systems*, vol. 1, no. 1, pp. 15–27, March 2014.

[8] ——, "Convex relaxation of optimal power flow—part II: Exactness," *IEEE Transactions on Control of Network Systems*, vol. 1, no. 2, pp. 177–189, June 2014.

[9] S. Sojoudi and J. Lavaei, "Physics of power networks makes hard optimization problems easy to solve," in *2012 IEEE Power and Energy Society General Meeting*, July 2012, pp. 1–8.

[10] M. Farivar and S. H. Low, "Branch flow model: Relaxations and convexification—part II," *IEEE Transactions on Power Systems*, vol. 28, no. 3, pp. 2565–2572, Aug 2013.

[11] R. Madani, S. Sojoudi, and J. Lavaei, "Convex relaxation for optimal power flow problem: Mesh networks," *IEEE Transactions on Power Systems*, vol. 30, no. 1, pp. 199–211, Jan 2015.

[12] J. Lavaei, D. Tse, and B. Zhang, "Geometry of power flows and optimization in distribution networks," *IEEE Transactions on Power Systems*, vol. 29, no. 2, pp. 572–583, March 2014.

[13] B. Kocuk, S. S. Dey, and X. A. Sun, "Inexactness of sdp relaxation and valid inequalities for optimal power flow," *IEEE Transactions on Power Systems*, vol. 31, no. 1, pp. 642–651, Jan 2016.

[14] L. Gan and S. H. Low, "Optimal power flow in direct current networks," *IEEE Transactions on Power Systems*, vol. 29, no. 6, pp. 2892–2904, Nov 2014.

[15] J. Li, F. Liu, Z. Wang, S. H. Low, and S. Mei, "Optimal power flow in stand-alone dc microgrids," *IEEE Transactions on Power Systems*, vol. 33, no. 5, pp. 5496–5506, Sep. 2018.

[16] J. Rimez and R. Belmans, "A combined ac/dc optimal power flow algorithm for meshed ac and dc networks linked by vsc converters," *International Transactions on Electrical Energy Systems*, vol. 25, no. 10, pp. 2024–2035, June 2015.

[17] S. Bahrami, F. Therrien, V. W. S. Wong, and J. Jatskevich, "Semidefinite relaxation of optimal power flow for ac–dc grids," *IEEE Transactions on Power Systems*, vol. 32, no. 1, pp. 289–304, Jan 2017.

[18] A. Venzke and S. Chatzivasileiadis, "Convex relaxations of probabilistic ac optimal power flow for interconnected ac and hvdc grids," *IEEE Transactions on Power Systems*, vol. 34, pp. 2706–2718, July 2019.

[19] M. Baradar, M. R. Hesamzadeh, and M. Ghandhari, "Second-order cone programming for optimal power flow in vsc-type ac-dc grids," *IEEE Transactions on Power Systems*, vol. 28, pp. 4282–4291, Nov 2013.

[20] F. Zohrizadeh, M. Kheirandishfard, E. Q. Jnr, and R. Madani, "Penalized parabolic relaxation for optimal power flow problem," in *2018 IEEE Conference on Decision and Control (CDC)*, Dec 2018, pp. 1616–1623.

[21] H. Ergun, J. Dave, D. Van Hertem, and F. Geth, "Optimal power flow for ac–dc grids: Formulation, convex relaxation, linear approximation, and implementation," *IEEE Transactions on Power Systems*, vol. 34, no. 4, pp. 2980–2990, July 2019.

[22] W. Feng, L. A. Tuan, L. B. Tjernberg, A. Mannikoff, and A. Bergman, "A new approach for benefit evaluation of multiterminal vsc–hvdc using a proposed mixed ac/dc optimal power flow," *IEEE Transactions on Power Delivery*, vol. 29, no. 1, pp. 432–443, Feb 2014.

[23] Z. Yang, H. Zhong, A. Bose, Q. Xia, and C. Kang, "Optimal power flow in ac–dc grids with discrete control devices," *IEEE Transactions on Power Systems*, vol. 33, no. 2, pp. 1461–1472, March 2018.